MEMORANDUM REPORT BRL-MR-3807

BRL

APPROXIMATE ANALYSIS FOR THE FORMATION OF ADIABATIC SHEAR BANDS

THOMAS W. WRIGHT

JANUARY 1990

U.S. ARMY LABORATORY COMMAND

BALLISTIC RESEARCH LABORATORY
ABERDEEN PROVING GROUND, MARYLAND

DESTRUCTION NOTICE

Destroy this report when it is no longer needed. DO NOT return it to the originator.

Additional copies of this report may be obtained from the National Technical Information Service. U.S. Department of Commerce, Springfield, VA 22161.

The findings of this report are not to be construed as an official Department of the Army position, unless so designated by other authorized documents.

The use of trade names or manufacturers' names in this report does not constitute indorsement of any commercial product.

REPORT DOCUMENTATION PAGE

Form Approved
OMB No. 0704-0168

1a REPORT SECURITY CLASSIFICATION UNCLASSIFIED	1b RESTRICTIVE MARKINGS
2a SECURITY CLASSIFICATION AUTHORITY	3 DISTRIBUTION / AVAILABILITY OF REPORT Approved for public release; distribution unlimited
2b DECLASSIFICATION / DOWNGRADING SCHEDULE	
4 PERFORMING ORGANIZATION REPORT NUMBER(S) BRL-MR-3807	5 MONITORING ORGANIZATION REPORT NUMBER(S)
6a NAME OF PERFORMING ORGANIZATION Ballistic Research Laboratory 6b OFFICE SYMBOL (If applicable) SLCBR-TB	7a NAME OF MONITORING ORGANIZATION
6c ADDRESS (City, State, and ZIP Code) Aberdeen Proving Ground, MD 21005-5066	7b ADDRESS (City, State, and ZIP Code)
8a NAME OF FUNDING / SPONSORING ORGANIZATION 8b OFFICE SYMBOL (If applicable)	9 PROCUREMENT INSTRUMENT IDENTIFICATION NUMBER
8c ADDRESS (City, State, and ZIP Code)	10 SOURCE OF FUNDING NUMBERS PROGRAM ELEMENT NO. / PROJECT NO. / TASK NO. / WORK UNIT ACCESSION NO.

11 TITLE (Include Security Classification)

APPROXIMATE ANALYSIS FOR THE FORMATION OF ADIABATIC SHEAR BANDS

12 PERSONAL AUTHOR(S)

WRIGHT, THOMAS W.

13a TYPE OF REPORT	13b TIME COVERED	14 DATE OF REPORT (Year, Month, Day)	15 PAGE COUNT
BRL Memorandum Report	FROM _____ TO _____		

16 SUPPLEMENTARY NOTATION

17 COSATI CODES			18 SUBJECT TERMS (Continue on reverse if necessary and identify by block number)
FIELD	GROUP	SUB-GROUP	adiabatic shear, [illegible]
11	06		
20	11		

19 ABSTRACT (Continue on reverse if necessary and identify by block number)

Parametric solutions are given for the formation of adiabatic shear bands in the context of the one-dimensional, nonlinear theory where inertia and elasticity are ignored. When heat conduction is also ignored, the exact solution reduces completely to a sequence of quadratures. For a perfectly plastic material with heat conduction, an implicit parametic solution is also constructed. This is similar to the previous one in many ways, but now it involves two quadratures; a single, nonautonomous, first-order ODE; and two functions that obey heat equations. This solution appears to be very accurate (compared to the full-finite element solution) until the time of stress collapse. Results indicate that for weak rate hardening of the power-law type, intense localization depends strongly on the intial characteristics. Within the context of rigid/perfect plasticity, a scaling law for the critical strain is given, and a figure of merit is defined that ranks materials according to their tendency to form adiabatic shear bands.

20 DISTRIBUTION / AVAILABILITY OF ABSTRACT ☒ UNCLASSIFIED/UNLIMITED ☐ SAME AS RPT ☐ DTIC USERS	21 ABSTRACT SECURITY CLASSIFICATION UNCLASSIFIED
22a NAME OF RESPONSIBLE INDIVIDUAL THOMAS W. WRIGHT	22b TELEPHONE (Include Area Code) 301/278-6046 22c OFFICE SYMBOL SLCBR-TB-W

DD Form 1473, JUN 86 *Previous editions are obsolete.*

INTENTIONALLY LEFT BLANK.

TABLE OF CONTENTS

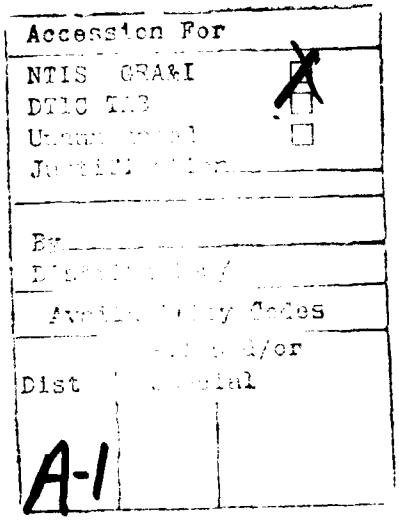

INTENTIONALLY LEFT BLANK.

LIST OF FIGURES

INTENTIONALLY LEFT BLANK.

ACKNOWLEDGMENT

My deepest thanks to Professor E. Varley of Lehigh University, who, as mentor and friend, reminded me of the effectiveness of parametric solutions and transformations of variables.

INTENTIONALLY LEFT BLANK.

1. INTRODUCTION AND EQUATIONS OF MOTION

Recent papers on the mechanics and mathematical analysis of the formation of adiabatic shear bands (Molinari and Clifton [1987] and Tzavaras [1987]) have emphasized the late-time, high-temperature behavior of the equations for thermo/visco/plasticity in order to judge whether or not a band will form from a small inhomogeneity. In fact, although the mathematical arguments presented in those papers are undoubtedly correct, they are misleading in that computational experience clearly shows that shear bands form at intermediate times somewhat after instability first occurs, but when the temperature in the band is still relatively low. It is the purpose of this paper to develop methods whereby the time of intense localization (not the time at onset of instability) can be calculated or at least estimated and to examine the causes of band formation and the effects of the dominant parameters.

Consider simple shearing of a slab of rigid/plastic material of thickness τ and width 2H. The motion is assumed to be of the form

$$x = X + u(Y,t), \quad y = Y, \quad z = Z, \tag{1.0}$$

where x,y,z denote present position; X,Y,Z denote reference position; and t is time. This may thought of as an idealized version of the Kolsky bar experiment on a thin-walled tube where τ is the wall thickness and 2H is the gage length. In nondimensional form, the governing equations to be studied are

$$(\tau s)_{,y} = 0 \tag{2.1}$$

$$(\tau\vartheta)_{,t} = (\tau s)v_{,y} + k(\tau\vartheta_{,y})_{,y} \tag{2.2}$$

$$s = \kappa g(\vartheta)(v_{,y})^m \tag{2.3}$$

$$\kappa_{,t} = M(\kappa,\vartheta)sv_{,y} , \tag{2.4}$$

where $-1 \le y \le +1$, $0 \le t < \infty$, and the commas denote partial differentiation with respect to the indicated independent variable. The first equation represents balance of momentum in the quasi-static approximation where s is the shear stress. From finite element solutions, Wright and Walter [1987], it is known that this approximation is very accurate up to moderate strain rates. The second equation represents balance of energy where ϑ is temperature, measured from some convenient reference temperature; k is thermal conductivity; $v = u_{,t}$ is the particle velocity; and $v_{,y}$ is the velocity gradient or plastic strain rate since elasticity is ignored. The first term on the right

of Equation 2.2 is the heat source due to plastic work and the second accounts for heat conduction. The third equation gives the flow stress in terms of a work hardening parameter, κ; a thermal softening function, $g(\vartheta)$, which is assumed to be monotonically decreasing with $g(0) = 1$; and a rate hardening factor where m is the rate hardening exponent. The last equation is an evolution law for work hardening and simply states that the rate of hardening is proportional to the rate of plastic work where the factor of proportionality depends on the current values of κ and ϑ. The inclusion of τ in Equations 2.1 and 2.2 indicates that the balance laws have been integrated through the thickness. It is tacitly assumed that the field variables s, v, ϑ, and κ do not vary through the thickness and that τ varies only slowly with y.

The relationships between the nondimensional variables and the physical variables, indicated by overbars, are as follows:

$$y = \bar{y}/H \qquad t = \dot{\bar{\gamma}}_o \bar{t} \tag{3.1}$$

$$s = \bar{s}/s_o \qquad \vartheta = \bar{\rho} c \bar{\vartheta}/s_o \qquad v = \bar{v}/\dot{\bar{\gamma}}_o H \qquad \kappa = \bar{\kappa}/\kappa_o \tag{3.2}$$

$$k = \bar{k}/\bar{\rho} c H^2 \dot{\bar{\gamma}}_o \qquad \text{where } s_o = (b\dot{\bar{\gamma}}_o)^m \kappa_o \, . \tag{3.3}$$

In Equation 3 $\dot{\bar{\gamma}}_o$ is the nominal, applied strain rate; s_o is a characteristic stress given by Equation 3.3; $\bar{\rho}$ is density; c is heat capacity; κ_o is a characteristic value for the work hardening parameter, and b is a characteristic time for rate hardening. Note that the characteristic stress, which includes the rate factor $(b\dot{\bar{\gamma}}_o)^m$, has been chosen so that $s = 1$ when $\kappa = 1$, $\vartheta = 0$, and $v_{,y} = 1$. It is necessary to define one more parameter, namely

$$a = - g_{,\vartheta}(0) = \bar{a} s_o / \bar{\rho} c, \qquad \text{where } \bar{a} = -\bar{g}_{,\vartheta}(0), \tag{4.0}$$

and the subscript denotes differentiation with respect to the argument indicated. The form in which the equations have been written is suitable for examining the effect of various small defects, such as variations in wall thickness, variations in strength, or variations in initial temperature.

In all problems to be considered below the velocity is taken to be constant on the boundaries, which are assumed to be insulated so that the temperature gradient vanishes there.

2. EXACT RESULTS: NON-HEAT-CONDUCTING CASE

Molinari and Clifton [1987] have given the exact solution to the non-heat-conducting case when stress is prescribed on the boundary and an approximate solution for the case when velocity is prescribed. Here, the exact solution for the velocity boundary condition will be developed.

With k = 0 in Equation 2.2 the thickness τ factors out, and Equations 2.2 and 2.4 may be combined to give a differential equation connecting κ and ϑ;

$$\kappa_{,t} = M(\kappa,\vartheta)\vartheta_{,t} \ . \tag{5.0}$$

This implies that κ is only a function of ϑ (and y in inhomogeneous cases) $\kappa = \hat{\kappa}(\vartheta)$. In turn, this allows Equation 2.3 to be written

$$s = G(\vartheta)(v_{,y})^m, \tag{6.0}$$

where $G(\vartheta) = \hat{\kappa}(\vartheta)g(\vartheta)$, and the explicit y-dependence has been suppressed. The problem has been scaled so that G(0) = 1. It will be assumed that G has at most one local maximum for $\vartheta \geq 0$. Typically G will increase initially, reach a maximum, and then decrease as shown in Figure 1b. Combining Equations 2.2 and 2.3 gives

$$\vartheta_{,t} = (\tau s)^{(1+m)/m}\, G^{-1/m}\, \tau^{-(1+m)/m}. \tag{7.0}$$

Because of Equation 2.1, the term $(\tau s)^{(1+m)/m}$ is a function only of time, so that a new time scale T(t) can be defined by the ODE

$$dT/dt = (\tau s)^{(1+m)/m} \quad T(0) = 0. \tag{8.0}$$

Since the right hand side of Equation 8 is positive, T will increase monotonically. However, when a shear band forms, the stress decreases rapidly, and since (1+m)/m is large when m is small, T will increase extremely slowly once the band is well formed. Now the energy equation may be written

$$G^{1/m}\, \vartheta_{,T} = \tau^{-(1+m)/m}. \tag{9.0}$$

This has the solution

$$H(\vartheta) = T\,\tau^{-(1+m)/m} + H(\vartheta_o(y)), \tag{10.1}$$

$$\text{where } H(\vartheta) \equiv \int_0^{\vartheta} G^{1/m}\, d\vartheta. \tag{10.2}$$

Since G is positive, H is monotonically increasing and, thus, invertible. Therefore, ϑ is now known implicitly as a function of T and y.

$$\vartheta = \hat{\vartheta}\,(T,y). \tag{11.0}$$

From the velocity boundary condition and the constitutive relation in Equation 2.3, the traction can be found as a function of T

$$\int_0^1 v_{,y}\, dy = 1 = \int_0^1 (\tau s)^{1/m}(\tau G)^{-1/m}\, dy, \tag{12.0}$$

or since τs is independent of y,

$$(\tau s)^{-1/m} = \int_0^1 (\tau G)^{-1/m}\, dy, \tag{13.0}$$

which gives τs as a function of T. Finally, Equation 13 may be used in Equation 8, and the solution of a simple ODE by quadrature completes the problem.

In summary, then, once $G(\vartheta)$ has been found from the solution of Equation 5 and the definition $G = \hat{\kappa}\, g$, the solution in parametric form is obtained by performing the following quadratures in sequence:

$$H(\vartheta) = H(\vartheta_0(y)) + T\,\tau^{-(1+m)/m}; \tag{14.1}$$

$$(\tau s)^{-1/m} = \int_0^1 (\tau G)^{-1/m}\, dy; \tag{14.2}$$

$$t = \int_0^T (\tau s)^{-(1+m)/m}\, dT. \tag{14.3}$$

Note that Equation 14 does reduce to the homogeneous solution when $\vartheta_0 = 0$ and $\tau = 1$, since then with the aid of Equations 14.1 and 14.2 and the definition of H, Equation 14.3 reduces to $t = \int_0^{\vartheta} G^{-1}\, d\vartheta$, which can be obtained directly from Equation 2. Also $v_{,y} = 1$ and $s = G(\vartheta)$ in this case.

That Equation 14 gives localized solutions may easily be seen by the following qualitative argument for geometric or initial temperature imperfections. In Figure 1a for a non-work-hardening material, an arbitrary softening function g and g raised to the power 1/m are sketched. Since m is usually a small number (0.025 or smaller for many metals), the second curve drops rapidly toward zero. As a consequence, the integral of $g^{1/m}$, also shown in Figure 1a, starts at zero, then rises rapidly, and finally levels out into a plateau, which has been normalized to 1 in the Figure. The situation for a work-hardening material, shown in Figure 1b, is similar, except that in that case, the integral of $G^{1/m}$ rises slowly at first, then increases very rapidly near the maximum of G, and finally goes into a plateau. In the figure, all curves have been renormalized as required so that each has 1 as an upper bound.

First, suppose that $\tau = 1$ and ϑ_0 is some nonconstant function of y. Then the initial distribution of temperature corresponds to some initial distribution of H, as shown by the dark lines near the origin in Figure 1a. As time increases, T(t) increases also, but Equation 14.1 shows that for each value of y, H simply translates by the amount T, so that at some later time, H has the distribution shown by the dark lines near 0.5 and later still by the dark line near 1.0. In turn, these correspond to new distributions of ϑ as shown in the figure. Since the curve $H(\vartheta)$ turns over to the right, the ϑ distribution expands, and when the maximum value of H encounters the plateau, the distribution of ϑ expands wildly with the maximum value of ϑ occurring at the same location as initially. In general, the more sharply H turns onto the plateau, the more sharply will the maximum in ϑ rise, and the more peaked will the distribution in ϑ become.

The graphical interpretation for the work-hardening case, shown in Figure 1b, is identical. Now, however, because $H(\vartheta)$ first turns up, the temperature distribution first becomes more compressed than initially. This has been noted by Burns [1989] in a completely different analysis. After G passes its maximum, and the H curve begins to turn to the right, the temperature distribution can expand, and finally it will peak sharply, just as before, when the maximum temperature moves onto the plateau.

The graphical interpretation is slightly different for mechanical imperfection with zero initial temperature. In this case, with τ nearly equal to 1 but varying slightly with y, the H distribution begins at zero, as indicated by the dots at the origin in Figure 1b, but according to Equation 14.1, it expands linearly with T as the whole pattern moves up the H axis. Correspondingly, the ϑ distribution starts at zero and spreads very slowly, as indicated in Figure 1b. The process continues until the maximum value of H reaches the plateau, which occurs at the location of the initial minimum in ϑ. As with the case of an initial temperature imperfection, the temperature distribution

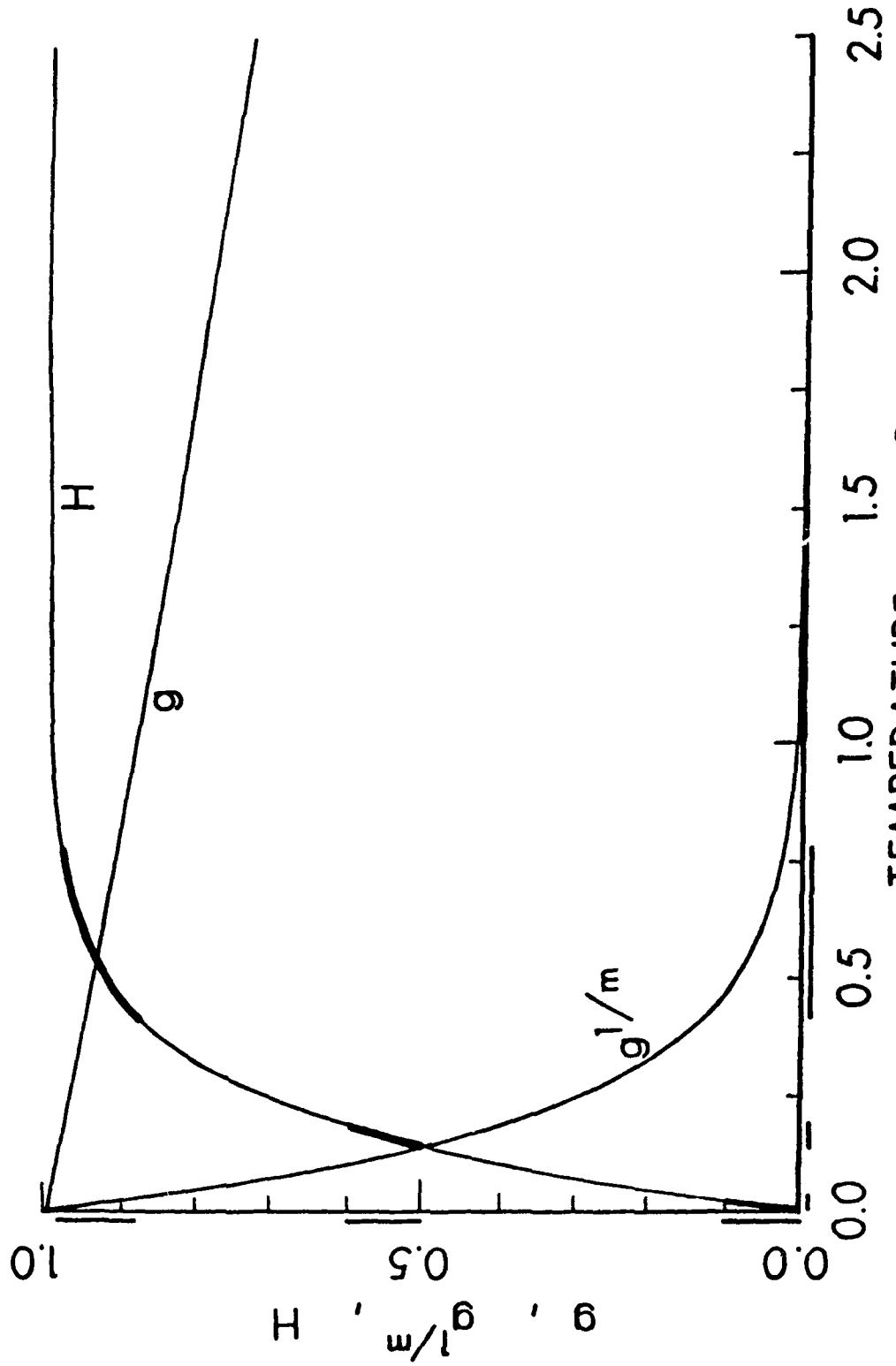

Figure 1a. Sketch of typical softening function g, $g^{1/m}$, $H = \int_0^{\Theta} g^{1/m}\, d\vartheta$ for a perfectly plastic material.

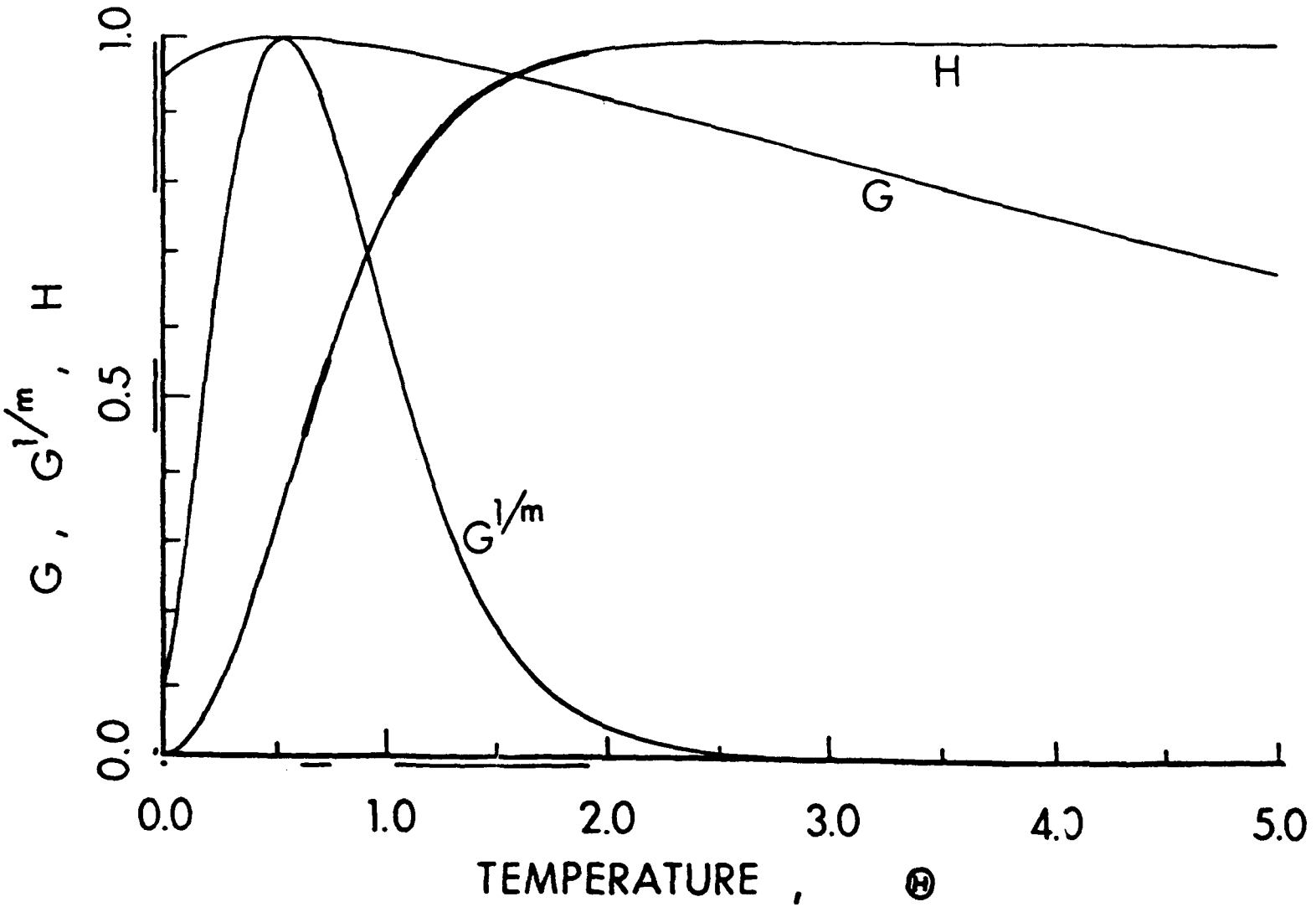

Figure 1b. Sketch of a typical composite-hardening/softening function G, $G^{1/m}$, $H = \int_0^{\vartheta} G^{1/m}\, d\vartheta$ for a work-hardening, thermal-softening material.

is compressed where $H(\vartheta)$ turns up and expands and peaks up sharply when $H(\vartheta)$ reaches the plateau.

3. ASYMPTOTIC RESULTS: THE EFFECT OF HEAT CONDUCTION

The result outlined above, which is exact if the thermal conductivity is zero, gives only a minimum value for the critical strain when there is finite conductivity. In fact, it is more accurate to refer to a critical temperature than to a critical strain. Criticality is reached when the maximum temperature is large enough to force the H function onto the plateau. Since the maximum temperature generally occurs in a narrow region with large temperature gradients on either side, heat conduction has the effect of delaying the critical condition by chopping off the peak and spreading the thermal energy to the sides. This effect was clearly seen in the finite element calculations reported by Wright and Walter [1987] and plotted in their Figure 8, replotted here in Figure 2. The left-hand side of the figure rises above the minimum as the nominal strain rate decreases. Since the nondimensional thermal conductivity varies inversely with the nominal strain rate (see Equation 3), this corresponds to a relative increase in the effect of heat conduction. The fact that the right-hand side of the figure rises above the minimum with increasing strain rate is thought to be an inertial effect and is still not understood in detail. Since this paper deals only with the quasi-static approximation, the right half of the curve will not be discussed further here, and all results obtained below will apply only to the left-hand side.

Only the rigid, perfectly plastic case will be examined, but the defect that sets off the localization may occur in the thickness, the initial strength, or the initial temperature distribution,

$$\tau = 1 + \delta(y) \quad , \quad \kappa = 1 + \lambda(y) \quad , \quad \vartheta_0 = \vartheta_0(y), \tag{15.0}$$

where $\max(|\delta|,|\lambda|,|\vartheta_0|) \ll 1$. In the cases to be considered, there is no work hardening so κ does not evolve. Consequently, only Equations 2.1, 2.2, and 2.3 apply.

The analysis in Section 2 introduced a second time scale, T(t), through the differential transformation of Equation 8. Since it turned out that T was the dominant time scale in the absence of heat conduction, which is regarded as only a small perturbing effect in the present case, the same transformation will be used here. Equation 2 becomes

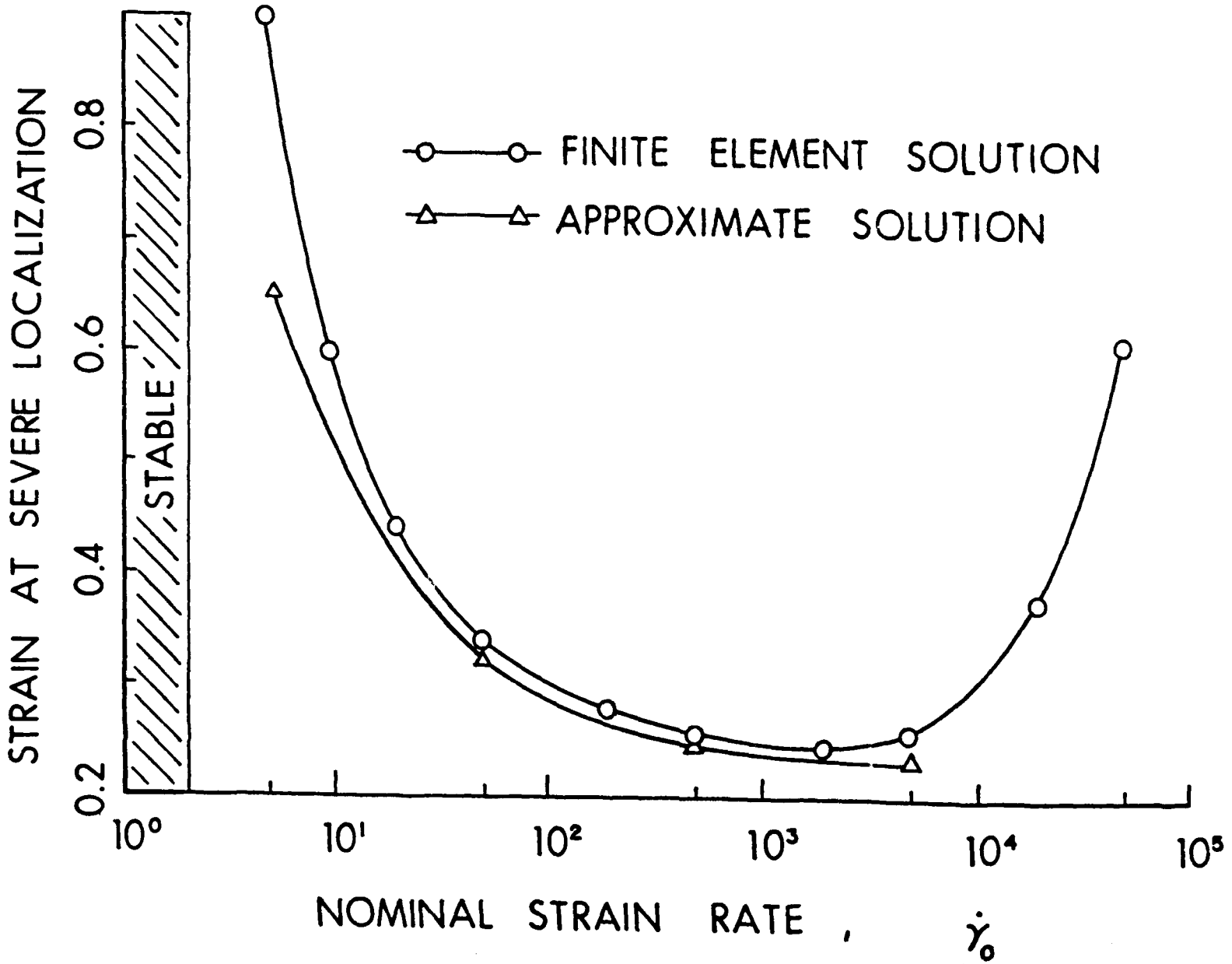

Figure 2. Strain at severe localization for the initial temperature defect $\vartheta_o = 0.1(1-y^2)^9 e^{-5y^2}$ as computed by finite elements, Wright and Walter [1987], and by the approximate method using Equations 25 and 17.

$$(\tau s)_{,y} = 0 \tag{16.1}$$

$$s = \kappa g(\vartheta)(v_{,y})^m \tag{16.2}$$

$$\tau\vartheta_{,T} = (\tau\kappa g)^{-1/m} + k\,\frac{dt}{dT}\,(\tau\vartheta_{,y}),y, \tag{16.3}$$

where as before

$$\frac{dT}{dt} = (\tau s)^{(1+m)/m} \tag{17.1}$$

$$(\tau s)^{-1/m} = \int_0^1 (\tau\kappa g)^{-1/m}\,dy. \tag{17.2}$$

Next transform the dependent variable using Equation 10.2 and rewrite the energy Equation 16.3 in terms of H.

$$\tau H_{,T} = (\tau\kappa)^{-1/m} + k\,\frac{dt}{dT}\left[(\tau H_{,y})_{,y} - \tau\,\frac{H''}{H'^2}\,h_y^2\right]. \tag{18.0}$$

Upon ignoring the last term, which is nonlinear in H, the equation may be written

$$\tau(H\text{-}fT)_{,T} = k\,\frac{dt}{dT}\,[\tau(H\text{-}fT)_{,y} + \tau f_{,y}T]_{,y}, \tag{19.1}$$

or

$$\tau(H\text{-}fT)_{,t} = k\,[\tau(H\text{-}fT)_{,y} + \tau f_{,y}T]_{,y}, \tag{19.2}$$

where

$$f \equiv \tau^{-(1+m)/m}\kappa^{-1/m}. \tag{19.3}$$

Equation 19.2 has the solution

$$H = fT + \beta, \tag{20.0}$$

where β satisfies an inhomogeneous heat equation with a source,

$$\tau\beta_{,t} = k(\tau\beta_{,y})_{,y} + k(\tau f_{,y})_{,y}T, \tag{21.1}$$

$$\beta(y,0) = H(\vartheta_0),\quad \beta_{,y} = -\,f_{,y}T \text{ on the boundaries.} \tag{21.2}$$

Since λ, δ, and ϑ_0 in Equation 15 have all been assumed to be small, the initial value of β is also small, and as a good approximation, Equation 21 may be replaced by

$$\beta_{,t} = k(\beta_{,yy} + Tf_{,yy}). \tag{22.0}$$

It is convenient to split β into two unknown functions. To that end, let $\beta = (\phi - f)T + r$, where ϕ satisfies

$$\phi_{,t} = k\phi_{,yy} \tag{23.1}$$

$$\phi(y,0) = f,\ \phi_{,y} = 0 \text{ on the boundaries,} \tag{23.2}$$

and f is defined as in Equation 19.3. Then the residual r must satisfy

$$r_{,t} = kr_{,yy} + \frac{dT}{dt}(f - \phi) \tag{24.1}$$

$$r(y,0) = H(\vartheta_0(y)) \quad \text{and } r_{,y} = 0 \text{ on the boundaries.} \tag{24.2}$$

Since $f - \phi$ is zero initially and $\frac{dT}{dt}$ tends to zero as t increases, the source term in Equation 24 is very weak. The Fourier components of r have the representation

$$r_n = f_n\, e^{-k(n\pi)^2 t} \int_0^t \frac{dT}{dt}\,(e^{k(n\pi)^2 t'} - 1)\, dt' + r_{n_o}\, e^{-k(n\pi)^2 t},$$

At early times, $r = 0(kt^2)$ for all n since $\frac{dT}{dt}$ is 1 initially. If $\frac{dT}{dt}$ is bounded by $e^{-\mu t}$ for some μ, then $r_n \to 0$ as $t \to \infty$. Thus, r_n is a small term. Finally, H has the representation

$$H(\vartheta) = \phi T + r\ , \tag{25.0}$$

where ϕ and r satisfy Equations 23 and 24. The problem is completed by first performing the integration in Equation 17.2, which yields a function of T and t, and then solving the ODE in Equation 17.1.

As a first example, consider the same problem considered by Wright and Walter [1987] with results plotted in Figure 2. That is let $\kappa = 1$ and $\vartheta_0(y) = 0.1(1-y^2)^9 e^{-5y^2}$. Then $\phi = f = 1$, and the source term in Equation 24.1 vanishes. Figure 3 shows the calculated response for a nominal strain rate of $50s^{-1}$. This result is typical. Stress follows nearly parallel to the unperturbed response initially, but then falls off as the temperature and strain rate in the shear band accelerate sharply. the strain at intense localization is taken at the point of maximum rate of increase of strain rate in the center of the band. This is the same criterion as used previously. The solution that follows from Equation 25 turns onto a plateau at late times in the same manner as the full, finite element solution, but the plateau occurs too soon so that maximum values of temperature and strain rate are underestimated and stress does not drop far enough. The early plateau occurs because H'' in Equation 18 is always negative and hence, the final omitted term in Equation 18 is positive, which would have the effect of requiring larger negative curvature in the next to last term to balance it in

the exact solution. Therefore, the error in the solution of Equation 25 becomes unacceptably large sometime before the final plateau is reached. The criterion for critical strain stated above was used to obtain the approximate points plotted in Figure 2. Clearly, the approximate solution gives a very good estimate of the critical strain over several orders of magnitude of nominal strain rate. At the lowest rates, the approximate solution loses accuracy because heat conduction is not sufficiently accounted for, and at the highest rates, it loses accuracy because inertia terms are ignored.

As a second example, consider a specimen with a thickness defect $\tau = 1 - \lambda(1-y^2)^9 e^{-5y^2}$. Results for $\lambda = 0.01$ and $\lambda = 0.001$ are shown in Figure 4. The group of three solid curves on the left all have the same defect and show that increasing nominal strain rate decreases the critical strain, which is qualitatively the same as for temperature defects. The right-hand curve shows that a smaller defect increases the critical strain. Finally, the dashed curve shows the effect of ignoring the source term in Equation 24, which in this case makes the residual identically zero. Figure 5 shows the calculated residual for the case $\lambda = 0.01$, $\dot{\gamma}_0 = 50s^{-1}$. Note that the maximum is less than $3x10^{-3}$. For the same defect, but with $\dot{\gamma}_0 = 500s^{-1}$, the residual has the same shape, but is an order of magnitude smaller everywhere.

4. UNIVERSAL SOLUTION AND SCALING LAW

Equations 10.2 and 18 provide the basis for obtaining considerable further insight into the localization process when m is a small parameter, which is usually the case. Begin by defining a new variable z

$$z = - m \ln \frac{g^{1/m} - g_\infty^{1/m}}{1 - g_\infty^{1/m}}, \tag{26.0}$$

where g_∞ is the limit of g as ϑ becomes large. Then use Laplace's method on Equation 10.2 in the form

$$H = \int_0^z \left[g^{1/m}_\infty + (1 - g^{1/m}_\infty)\, e^{-z'/m} \right] \frac{d\vartheta}{dz'}\, dz'. \tag{27.0}$$

Assume that $d\vartheta/dz$ can be expressed as a power series in z, $d\vartheta/dz = a_0 + a_1 z + a_2 z^2 + \ldots$ where the coefficients a_0, a_1, ... are found from Equation 26 by expressing g as a function of z, differentiating with respect to z and evaluating at $z = 0$.

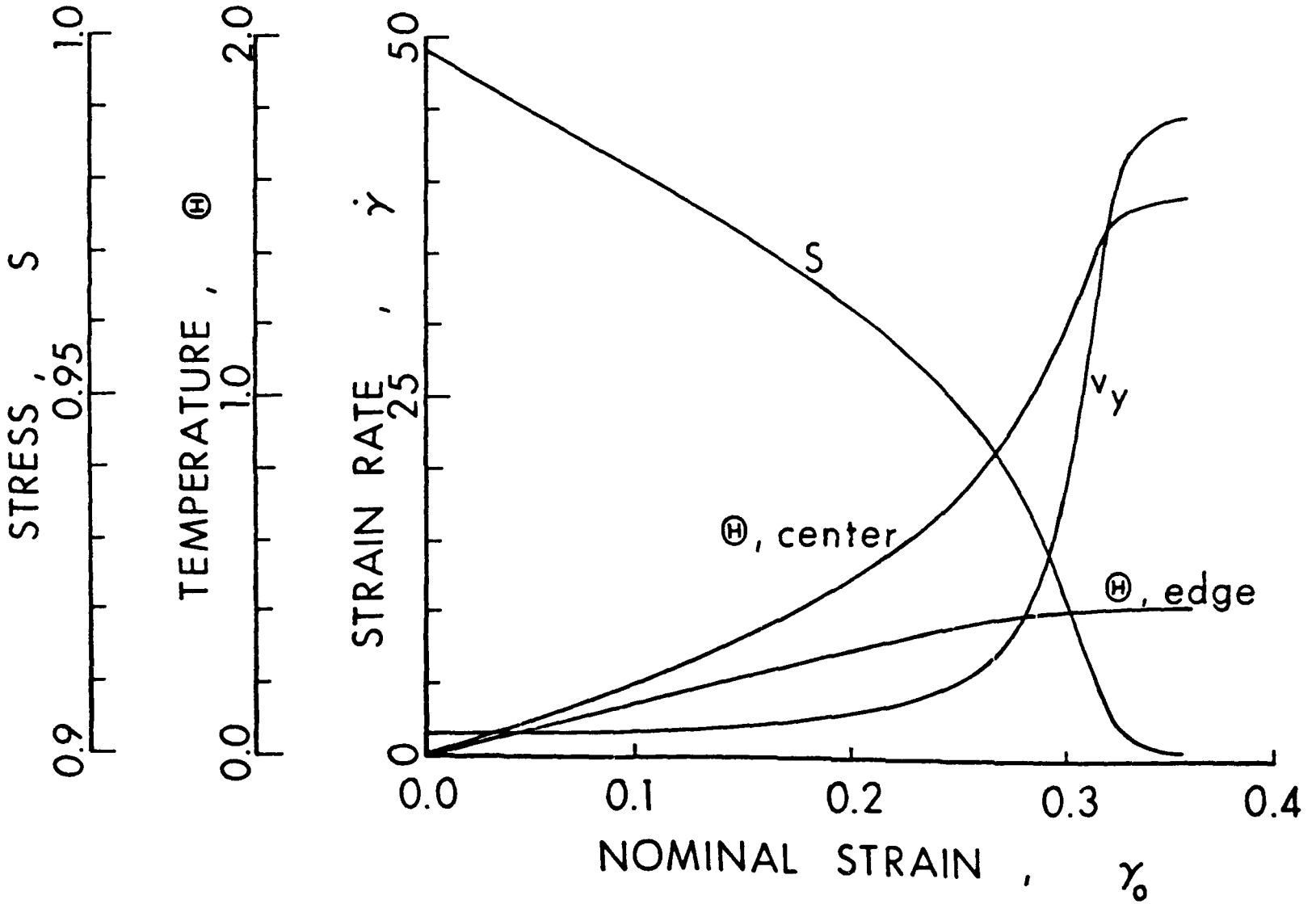

Figure 3. Typical response as calculated by the approximate method using Equations 25 and 17 for a temperature defect.

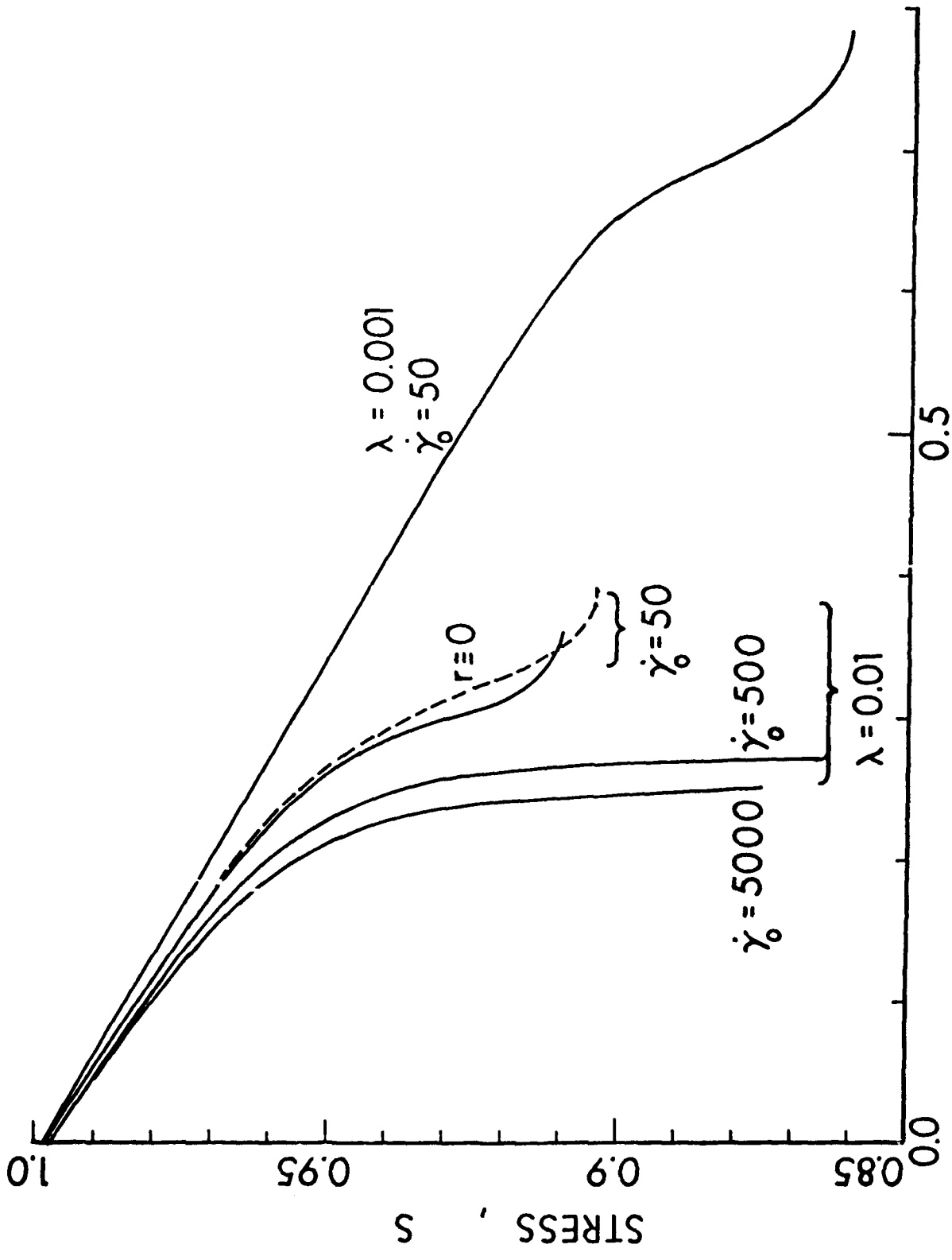

Figure 4. Comparison of responses for mechanical defects as calculated by the approximate method using Equations 25 and 17 for various conditions.

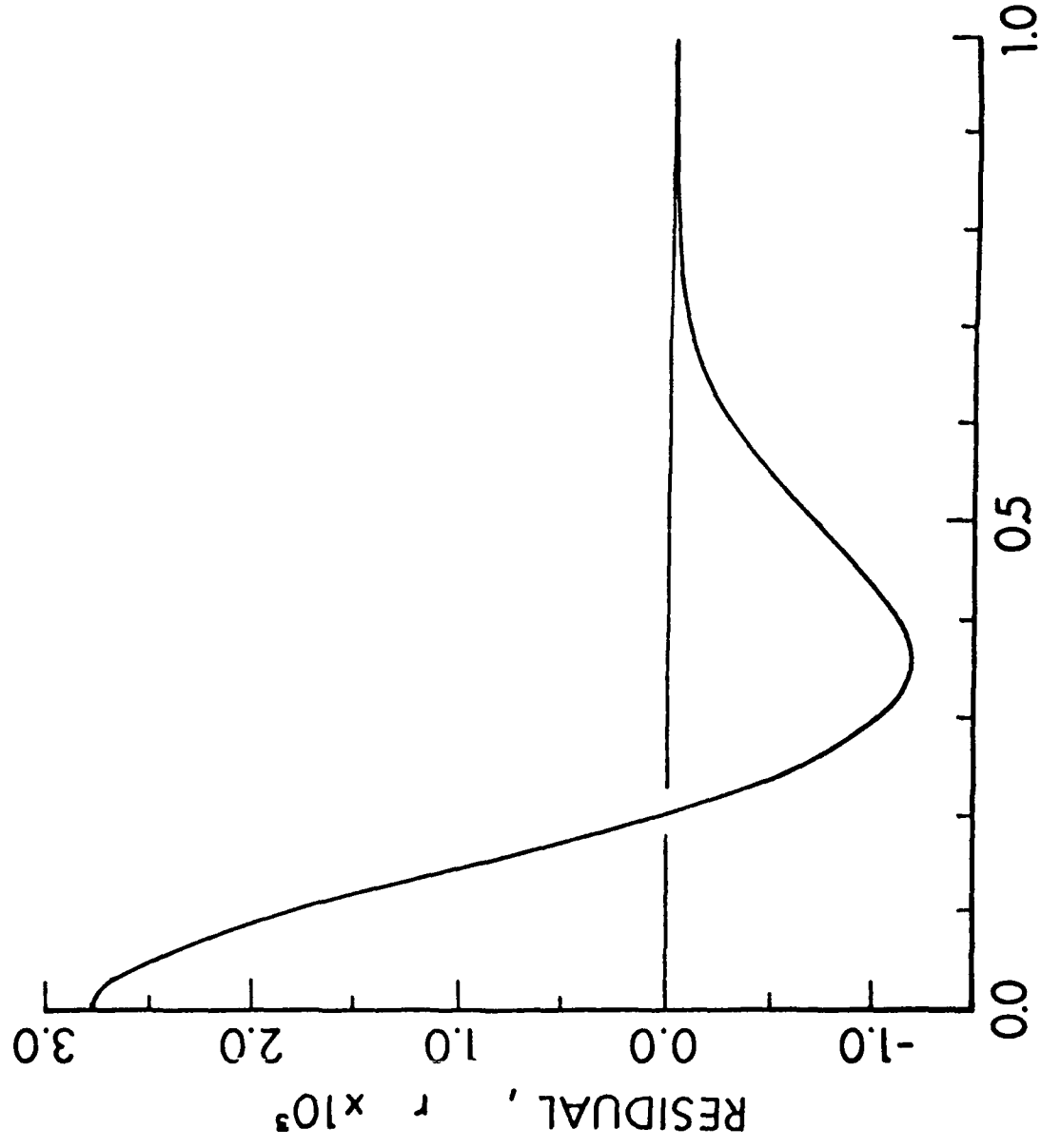

Figure 5. The residual function for a typical case.

$$a_0 = \frac{d\vartheta(0)}{dz} = - \frac{(1-g_\infty^{1/m})}{g'(0)} \approx a^{-1} \tag{28.1}$$

$$a_1 = \frac{d^2\vartheta(0)}{dz^2} = - \frac{1}{g'(0)} \left[- \frac{1-g_\infty^{1/m}}{m} + \frac{1-m}{m} \left(1-g_\infty^{1/m}\right)^2 + \right.$$

$$\left. + \left(\frac{1-g_\infty^{1/m}}{g'(0)}\right)^2 g''(0) \right] \tag{28.2}$$

$$\approx a^{-1} \left(-1 + \frac{g''(0)}{a^2}\right), \text{ etc.} \tag{28.3}$$

When evaluated term by term, the integral in Equation 27 gives

$$H = g_\infty^{1/m}\ \vartheta + (1-g_\infty^{1/m})[m(1-e^{-z/m})(a_0 + ma_1 + 2m^2a_2 + \ldots) + mze^{-z/m}(a_1 + 2ma_2 + \ldots) + mz^2e^{-z/m}\ (a_2 + \ldots) + 0\ (mz^ne^{-z/m})]. \tag{29.0}$$

Since m is small, the terms in $mz^ne^{-z/m}$ will be ignored at all orders of n so that a good approximation for H is

$$H \approx g_\infty^{1/m}\ \vartheta + \frac{mC}{a}\ (1 - g_\infty^{1/m}), \tag{30.0}$$

where Equation 26 has been used, and C is a constant chosen so that $H - g_\infty^{1/m}\,\vartheta$ takes on appropriate values as ϑ tends toward infinity (assuming that $\int_0^\infty \left[g^{1/m} - g_\infty^{1/m}\right] d\vartheta$ converges). For small m, $g_\infty^{1/m}$ may be extremely small. For example, if $g_\infty = 0.5$ and $m = 0.025$, then $g_\infty^{1/m} \approx 10^{-12}$, which for all practical purposes may be set equal to zero. When that is done, H takes on the simple form

$$H = \frac{mC}{a}\ (1-g^{1/m}). \tag{31.0}$$

With $g = \exp(-a\vartheta)$, this is exact, and C = 1. Plots of H, according to Equation 31 or the exact expression in Equation 10.2, are indistinguishable for reasonable choices for g such as $g = 1 - a\vartheta$ or $g = 1/2\ (1 + e^{-2a\vartheta})$.

Now, from the definition of H in Equation 10.2 together with Equation 31,

$$H'(\vartheta) = g^{1/m} = 1 - \frac{H}{mC/a} \tag{32.1}$$

and

$$H''(\vartheta) = -\frac{a}{mC^2}\left(1 - \frac{H}{mC/a}\right), \tag{32.2}$$

so that, after a simple linear rescaling,

$$\hat{H} = \frac{H}{mC/a}, \hat{T} = \frac{T}{mC/a}, \hat{t} = \frac{t}{mC/a}, \hat{k} = \frac{mC}{a}\, k. \tag{33.0}$$

The basic Equation 18 may be written as

$$\tau\hat{H}_{,\hat{T}} = (\tau\kappa)^{-1/m} + \hat{k}\,\frac{d\hat{t}}{d\hat{T}}\left[(\tau\hat{H}_{,y})_{,y} + \tau\frac{(\hat{H}_{,y})^2}{1-\hat{H}}\right]. \tag{34.0}$$

This is a universal approximate equation for $\hat{H}$ no matter what the softening function $g(\vartheta)$ may be. Since $d\hat{t}/d\hat{T}$ is given by Equation 17.1, and from Equation 31, it is known that the expression $g^{1/m} = 1/(1 - \hat{H})$ is a good approximation; Equation 17.2 may now be rewritten as

$$\frac{dt}{d\hat{T}} = \frac{mC}{a}\left[\int_0^1 \frac{(\tau\kappa)^{-1/m}}{1 - \hat{H}}\, dy\right]^{1+m}. \tag{35.0}$$

Equations 34 and 35 imply that all effects of the defect, whether in τ, κ, or ϑ_o, are carried by the universal function $\hat{H}$.

Furthermore, since Equation 35 shows that, for a given defect in different materials, the critical time and, hence, the critical strain, scales according to the ratio mC/a (with some additional minor modification due to rescaled thermal conductivity); it is clear that the primary influence of the thermal softening function is through its initial slope only (recall that $a = -g'(0)$). The only effect of the exact shape of $g(\vartheta)$ comes through the coefficient C, which may be expected to have values $C = 1 + 0(m)$, according to Equation 29.

Contrary to the emphasis placed on the behavior at large temperatures by Molinari and Clifton [1987] in proposing their L_* criterion for severe localization, the present analysis makes clear that it is the early behavior of the softening function that determines when localization will occur. After

all, large temperature changes occur during localization, not before. In fact, the temperature required to carry H to .99mC/a (ie., 99% of the plateau value) is rather modest for reasonable softening functions. From Equation 31, at this value of H, g has the value $(.01)^m$, which decreases from about .955 to .891 as m increases from .01 to .025. Then, for reasonable functions such as $1 - a\vartheta$, $e^{-a\vartheta}$, or $1/2\ (1 + e^{-2a\vartheta})$, all of which have the same initial slope, $a\vartheta$ varies from about .045 to .047 for m = .01 and from about .109 to .123 for m = .025. Notice that since g is so close to 1, m and the initial slope of g have more influence on the corresponding temperature than the exact form of the softening function. For high-strength steels ($\bar{\rho} \cong 7800$ kg/m^3, c ≅ 500 J/kg/°K, $\kappa_o \cong 0.5$ GPa), reasonable values of a are about 0.1, which translates into temperature increases when $\hat{H}$ reaches .99 of about 45°C for m = .01 and about 115°C for m = .025. These increases in temperature, reached just before intense localization, are small compared to those actually reached in typical, fully formed shear bands, Hartley, et al., [1987].

If $g_\infty \neq 0$, the L_∞ criterion of Molinari and Clifton [1987] indicates that localization is not to be expected because H has no limit as ϑ tends toward infinity. However, Equation 30 shows that this criterion is inadequate when m is small. In fact, full finite element solutions for the three softening functions $1-a\vartheta$, $e^{-a\vartheta}$, and $1/2\ (1 + e^{-2a\vartheta})$ all give approximately the same time for intense localization, Walter [1989]. The actual times are slightly more separated than predicted by the scaling mC/a, but the ordering is the same. Note that the L_∞ criterion predicts localization for the first two functions, but not for the third.

5. FURTHER APPROXIMATIONS FOR WEAK PERTURBATIONS

Suppose that the wall thickness τ, the strength κ, and the initial temperature ϑ_o all have a weak cosine variation over the width of the sheared section.

$$\tau = 1 - \delta \cos\pi y \tag{36.1}$$

$$\kappa = 1 - \lambda \cos\pi y \tag{36.2}$$

$$\vartheta_0 = \varepsilon \cos\pi y, \tag{36.3}$$

where $\delta/m << 1$, $\lambda/m << 1$, $a\varepsilon/m << 1$. Then good approximations to the solutions of Equations 23 and 24 are

$$\phi = 1 + \left(\frac{1+m}{m}\ \delta\ +\ \frac{1}{m}\ \lambda \right)\ e^{-\hat{\lambda}_n \hat{\gamma}_1} \cos\pi y \tag{37.1}$$

$$\hat{r} = \frac{a}{m}\ \varepsilon\ e^{-k\pi^2\hat{t}}\ \cos\pi y, \tag{37.2}$$

where r has been rescaled in Equation 25 to match $\hat{H}$ and $\hat{T}$, and the forcing function in Equation 24 has been ignored since it only gives rise to a small correction. Now the integral in Equation 35 may be written as

$$(\tau s)^{-1/m} = \frac{1}{1-\hat{T}} \int_0^1 \frac{dy}{(1-a\cos\pi y)(1-b\cos\pi y)(1-c\cos\pi)}, \tag{38.0}$$

where $a = \delta/m$, $b = \lambda/m$, and $c = \frac{e^{-k\pi^2\hat{t}}}{1-\hat{T}} \left[\frac{a}{m}\varepsilon + \hat{T}\left(\frac{1+m}{m}\delta + \frac{\lambda}{m}\right)\right]$, and $a,b,c < 1$ ($c<1$ can be justified *a posteriori*). After the change of variable $z = \cos\pi y$, Equation 38 is easily evaluated by considering the related contour integral with poles at $z = 1/a, 1/b, 1/c$ and a branch cut on $-1 \le z \le +1$. The result is

$$(\tau s)^{-1/m} = \frac{1}{1-\hat{T}} \left\{ \frac{a^2}{(b-a)(c-a)\sqrt{1-a^2}} + \frac{b^2}{(c-b)(a-b)\sqrt{1-b^2}} + \frac{c^2}{(a-c)(b-c)\sqrt{1-c^2}} \right\} \tag{39.0}$$

for $a \neq b \neq c$. To complete the solution Equation 39 (with the above values for a, b, and c restored) replaces the integral in Equation 35 to yield a nonautonomous ordinary differential equation in t and $\hat{T}$.

Rather than considering all three types of defect at once, it is instructive first to consider them one at a time.

i) Case 1: $\lambda = \delta = 0$, $\varepsilon \neq 0$. This is the simplest case. Equation 35 reduces to

$$\frac{d\hat{t}}{d\hat{T}} = \left[(1-\hat{T})^2 - \left(\varepsilon\frac{a}{m}e^{-k\pi^2\hat{t}}\right)^2\right]^{-(1+m)/2}. \tag{40.0}$$

In the limiting case of $\hat{k} \to 0$ and $m \ll 1$, so that m may be ignored in the exponent, Equation 40 may be integrated exactly to yield an estimate for the critical time (nondimensional) or critical strain

$$\gamma_{cr} = t_{cr} = \frac{mC}{a} \ln \left\{ \frac{1+\sqrt{1-(\varepsilon a/m)^2}}{\varepsilon a/m} \right\} \approx \frac{mC}{a} \ln \frac{2}{\varepsilon a/m} . \tag{41.0}$$

ii) Case 2: $\delta = \varepsilon = 0$, $\lambda \neq 0$. Equation 35 reduces to

$$\frac{d\hat{t}}{d\hat{T}} = \left\{ \frac{1 - \hat{T}\,(1-e^{-k\pi^2\hat{t}})}{\sqrt{1 - (\lambda/m)^2}} \cdot \frac{\left[\sqrt{(1-\hat{T})^2 - (\hat{T}\,\frac{\lambda}{m}\,e^{-k\pi^2\hat{t}})^2} + \sqrt{1 - (\lambda/m)^2}\,\hat{T}e^{-k\pi^2\hat{t}}\right]^{-1}}{\sqrt{(1 - \hat{T})^2 - (\hat{T}\,\frac{\lambda}{m}\,e^{-k\pi^2\hat{t}})^2}} \right\}^{1+m} . \tag{42.0}$$

As with case 1, in the limit of $\hat{k} \rightarrow 0$ and $m << 1$, so that m may be ignored in the final exponent, Equation 42 may be evaluated exactly to yield

$$\gamma_{cr} = t_{cr} = \frac{Cm}{a} \frac{1}{\sqrt{1 - (\lambda/m)^2}} \ln \frac{1 + \sqrt{1 - (\lambda/m)^2}}{\lambda/m} \cdot \frac{\sqrt{1+\lambda/m}}{\sqrt{1-\lambda/m}} . \tag{43.0}$$

$$\approx \frac{Cm}{a} \ln \frac{2}{\lambda/m}$$

iii) Case 3: $\lambda = \varepsilon = 0$, $\delta \neq 0$. This is exactly the same as Case 2 with λ/m replaced by $\delta(1+m)/m$.

To treat all three types of defect simultaneously, consider the following approximation for the integral in Equation 38.

$$\int_0^1 \frac{dy}{[1-(a+b+c)\cos\pi y]} = [1 - (a+b+c)^2]^{-1/2}. \tag{44.0}$$

Proceeding as before leads to the estimate

$$\gamma_{cr} = t_{cr} \approx \frac{mC}{a} \ln \frac{2}{\left(\varepsilon \frac{a}{m} + \frac{1+m}{m}\,\delta + \frac{\lambda}{m}\right)} . \tag{45.0}$$

Equations 41, 43, and 45 may be regarded as approximate scaling laws. Note that the dominant effect comes from the material properties mC/a and that the defect strength aε/m, λ/m, or δ(1+m)/m has only a logarithmic effect.

In evaluating Equation 40 with $\hat{k} = 0$, it is clear that t_{cr} occurs when the terms in brackets on the right-hand side vanish and $\hat{T} = 1 - \varepsilon a/m$. When $\hat{k} \neq 0$, Equation 40 must be evaluated numerically. It turns out $\hat{t}$ now has infinite range, and $\hat{T}$ is bounded by the curve $\hat{T} = 1 - \varepsilon \frac{a}{m} e^{-\lambda_n^2 \hat{t}}$, so it is not as easy as before to estimate the critical strain, which now must be found by actually computing the stress history and judging where stress collapse occurs. The other cases are analogous.

Figure 6 shows the stress response as calculated from Equations 42 and 44 with nonzero thermal conductivity. The solid curves used Equation 42, and the dotted curves used Equation 44. When the defect is small enough, Equation 44 seems to give a very good approximation. Also shown by the dashed line in the figure is the curve calculated from Equations 25, 17.2, and 17.1. The nominal strain rate for these curves is $50s^{-1}$. Although the solution for a mechanical defect has yet to be calculated by the full, finite element method, the previous results for a temperature defect give confidence that the dashed curves are accurate until the plateau is reached. The figure shows that Equation 42 overestimates the critical time at $50s^{-1}$, and that the error is smaller for smaller defects. The overestimate occurs because of the approximation $(1-a)^{1/m} \approx 1-a/m$ for $a/m << 1$, which is used in the integrand of Equation 35 in obtaining Equation 38. Finally the critical time, as calculated from Equation 43, is shown by the vertical interrupted lines. Clearly, the simple formula gives a very good estimate considering the complexity of the full calculation.

Equations 41 or 43 or 45 appear to give lower bounds, but that is not quite the case. Whereas ignoring heat conduction and m, in the final exponent 1+m, makes an underestimate of the critical strain, the approximation for $(1-a)^{1/m}$, as noted above, tends toward overestimation of the critical strain. Thus, the approximations tend to compensate each other to some extent, although for very small defects, the last approximation can be very accurate.

6. CONCLUSION

The approximate methods used in this paper reduce a complex calculation on a main frame or mini-computer to a relatively simple calculation on a micro-computer, since integration of the system in Equations 17, 23, 24, and 25 is easily accomplished with commercially available software

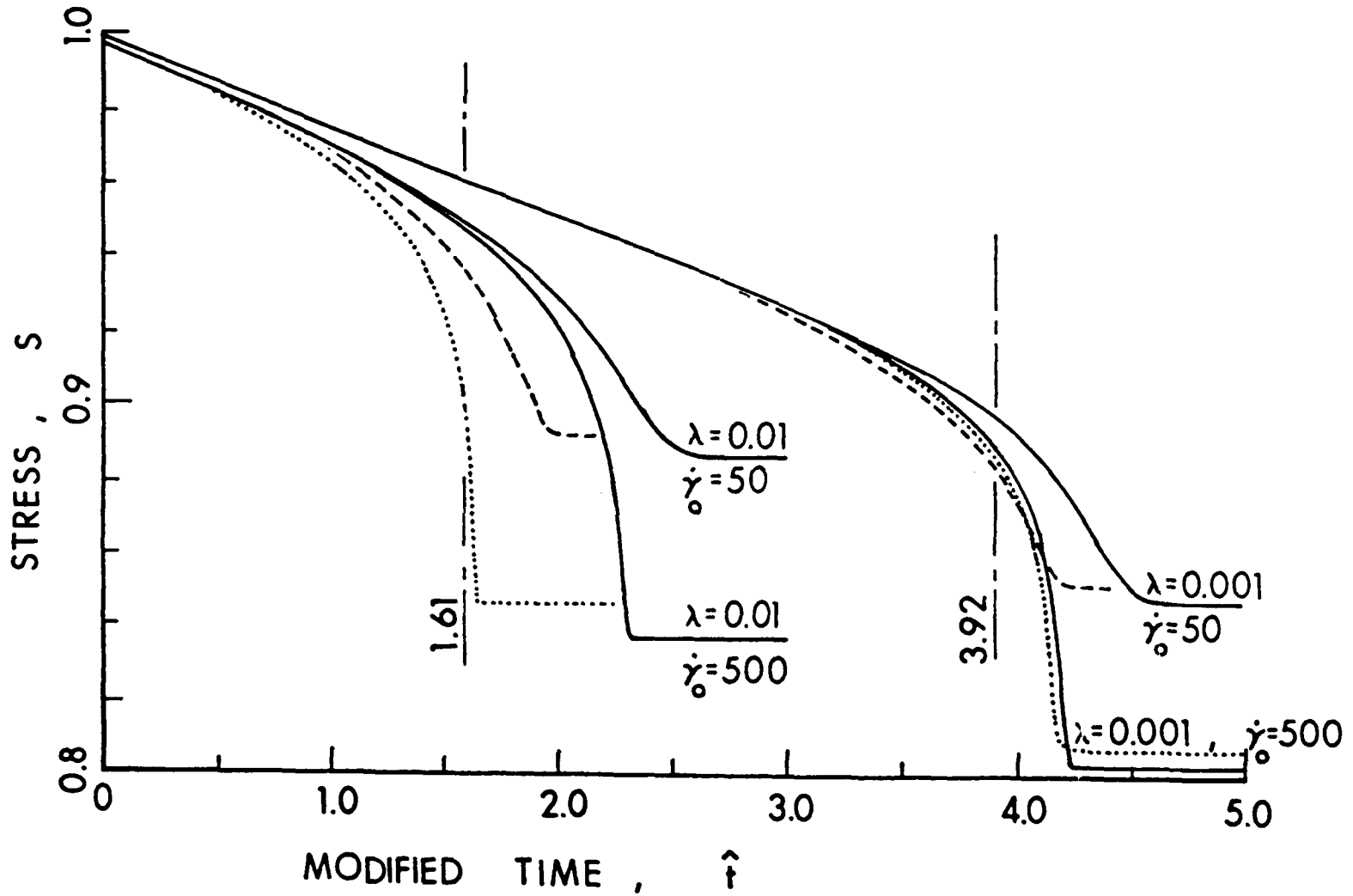

Figure 6. Comparison of responses for mechanical defects using various levels of approximation.

packages. The principal conclusion to be drawn is that localization depends strongly on the low-temperature thermal softening and on the rate sensitivity. In fact, because of its dominant effect on scaling, the ratio m/a should perhaps be regarded as a figure of merit that ranks perfectly/plastic materials according to their tendency to form adiabatic shear bands. The shape characteristic C has been omitted because its value is always near to one and would be difficult to determine experimentally in any case. The reciprocal of the ratio may be called "shear band susceptibility."

$$\chi_{SB} = a/m. \tag{46.0}$$

The susceptibility controls not only the critical strain, as has been demonstrated above, but in an earlier paper, Wright and Walter [1987], it was found to play a role in the criterion for absolute stability and in the early growth rate of unstable perturbations. Susceptibility does not tell the whole story, however, since the critical strain is also dependent on many other factors; among these are defect size and shape and thermal conductivity, whose effects have been considered above, and inertia, whose effect is yet to be explored.

7. REFERENCES

Burns, T.J. "Similarity and Bifurcation in Unstable Viscoplastic Shear," to appear SIAM Journal of Applied Math, 1989.

Hartley, K.A., Duffy, J., and Hawley, R.H. "Measurement of the Temperature Profile During Shear Band Formation in Steels Deforming at High Strain Rates," Journal of the Mechanics and Physics of Solids, 35, 283-301, 1987.

Molinari, A., and Clifton, R.J. "Analytical Characterization of Shear Localization in Thermoviscoplastic Materials," Journal of Applied Mechanics, 54, 806-812, 1987.

Tzavaras, A.E. "Effect of Thermal Softening in Shearing of Strain-Rate Dependent Materials," Archive for Rational Mechanics and Analysis, 99, 349-374, 1987.

Walter, J.W. Numerical Experiments on Adiabatic Shear Bands (in preparation, personal communication), 1989.

Wright, T.W., and Walter, J.W. "On Stress Collapse in Adiabatic Shear Bands," Journal of the Mechanics and Physics of Solids, 35, 701-720, 1987.

No of Copies	Organization
..., unlimited) 12	Administrator
..., limited) 2	Defense Technical Info Center
...ed) 2	ATTN: DTIC-DDA
	Cameron Station
	Alexandria, VA 22304-6145
1	HQDA (SARD-TR)
	WASH DC 20310-0001
1	Commander
	US Army Materiel Command
	ATTN: AMCDRA-ST
	5001 Eisenhower Avenue
	Alexandria, VA 22333-0001
1	Commander
	US Army Laboratory Command
	ATTN: AMSLC-DL
	Adelphi, MD 20783-1145
2	Commander
	Armament RD&E Center
	US Army AMCCOM
	ATTN: SMCAR-MSI
	Picatinny Arsenal, NJ 07806-5000
2	Commander
	Armament RD&E Center
	US Army AMCCOM
	ATTN: SMCAR-TDC
	Picatinny Arsenal, NJ 07806-5000
1	Director
	Benet Weapons Laboratory
	Armament RD&E Center
	US Army AMCCOM
	ATTN: SMCAR-CCB-TL
	Watervliet, NY 12189-4050
1	Commander
	US Army Armament, Munitions
	and Chemical Command
	ATTN: SMCAR-ESP-L
	Rock Island, IL 61299-5000
1	Commander
	US Army Aviation Systems Command
	ATTN: AMSAV-DACL
	4300 Goodfellow Blvd.
	St. Louis, MO 63120-1798
1	Director
	US Army Aviation Research
	and Technology Activity
	Ames Research Center
	Moffett Field, CA 94035-1099

No of Copies	Organization
1	Commander
	US Army Missile Command
	ATTN: AMSMI-RD-CS-R (DOC)
	Redstone Arsenal, AL 35898-5010
1	Commander
	US Army Tank-Automotive Command
	ATTN: AMSTA-TSL (Technical Library)
	Warren, MI 48397-5000
1	Director
	US Army TRADOC Analysis Command
	ATTN: ATAA-SL
	White Sands Missile Range, NM 88002-5502
(Class. only) 1	Commandant
	US Army Infantry School
	ATTN: ATSH-CD (Security Mgr.)
	Fort Benning, GA 31905-5660
(Unclass. only) 1	Commandant
	US Army Infantry School
	ATTN: ATSH-CD-CSO-OR
	Fort Benning, GA 31905-5660
(Class. only) 1	The Rand Corporation
	P.O. Box 2138
	Santa Monica, CA 90401-2138
1	Air Force Armament Laboratory
	ATTN: AFATL/DLODL
	Eglin AFB, FL 32542-5000

Aberdeen Proving Ground

Dir, USAMSAA
ATTN: AMXSY-D
AMXSY-MP, H. Cohen

Cdr, USATECOM
ATTN: AMSTE-TO-F

Cdr, CRDEC, AMCCOM
ATTN: SMCCR-RSP-A
SMCCR-MU
SMCCR-MSI

Dir, VLAMO
ATTN: AMSLC-VL-D

No of Copies	Organization
3	Director US Army Research Office ATTN: J. Chandra I. Ahmad J. Wu P.O. Box 12211 Research Triangle Park, NC 27709-2211
3	Director US Army BMD Advanced Technology Center ATTN: ATC-T/M. Capps ATC-RN/P. Boyd ATC-M/S. Brockway CRDABH-5/W. Loomis P.O. Box 1500, West Station Huntsville, AL 35807
1	Commander US Army Natick Research and Development Center ATTN: DRXRE/D. Sieling Natick, MA 01762
3	Director US Army Materials Technology Laboratory ATTN: SLCMT-MRD/J. Mescall S. Chou J. Dandekar Watertown, MA 021720-0001
2	Commander Armament RD&E Center US Army AMCCOM ATTN: SMCAR-CC/J. Corrie J. Beetle Picatinny Arsenal, NJ 07806-5000
1	Commander US Army Harry Diamond Laboratories ATTN: SLCHD-TA-L 2800 Powder Mill Road Adelphi, MD 20783
2	Office of Naval Research Dept. of the Navy ATTN: Y. Rajapakse A. Tucker Washington, DC 20360
1	Commander US Naval Air Systems Command ATTN: AIR-604 Washington, DC 20360
1	Commander Naval Sea Systems Command ATTN: Code SEA-62D Dept. of the Navy Washington, DC 20362-5101

No of Copies	Organization
3	Commander Naval Surface Warfare Center ATTN: W. Holt W. Mock Tech Library Dahlgren, VA 22448-5000
3	Commander Naval Surface Warfare Center ATTN: R. Crowe Code R32/S. Fishman Code X211/Library Silver Spring, MD 20902-5000
1	US Naval Academy Dept. of Mathematics ATTN: R. Malek-Madani Annapolis, MD 21402
4	Air Force Armament Laboratory ATTN: J. Foster J. Collins J. Smith G. Spitale Eglin AFB, FL 32542-5438
2	Air Force Wright Aeronautical Laboratories Air Force Systems Command Materials Laboratory ATTN: T. Nicholas J. Henderson Wright-Patterson AFB, OH 45433
2	Director Defense Advanced Research Projects Agency ATTN: Tech Info B. Wilcox 1400 Wilson Blvd. Arlington, VA 22209
7	Sandia National Laboratories ATTN: L. Davison P. Chen W. Herrman J. Nunziato S. Passman E. Dunn M. Forrestal P.O. Box 5800 Albuquerque, NM 87185-5800
1	Sandia National Laboratories ATTN: D. Bammann Livermore, CA 94550
1	Director National Aeronautics and Space Administration Lyndon B. Johnson Space Center ATTN: Library Houston, TX 77058

No of Copies	Organization
1	Director Jet Propulsion Laboratory ATTN: Library (TDS) 4800 Oak Grove Drive Pasadena, CA 91103
1	National Institute of Science and Technology ATTN: T. Burns Technology Building, Rm A151 Gaithersburg, MD 20899
1	Forestal Research Center Aeronautical Engineering Laboratory Princeton Unviersity ATTN: A. Eringen Princeton, NJ 08540
1	University of Missouri-Rolla Dept. of Mechanical and Aerospace Engineering ATTN: R. Batra Rolla, MO 65401-0249
1	California Institute of Technology Division of Engineering and Applied Science ATTN: J. Knowles Pasadena, CA 91102
1	Denver Research Institute University of Denver ATTN: R. Recht P.O. Box 10127 Denver, CO 80210
1	Massachusetts Institute of Technology Dept. of Mechanical Engineering ATTN: L. Anand Cambridge, MA 02139
2	Rennselaer Polytechnic Institute Dept. of Mechanical Engineering ATTN: E. Lee E. Krempl Troy, NY 12181
1	Rennselaer Polytechnic Institute Dept. of Computer Science ATTN: J. Flaherty Troy, NY 12181
5	Brown University Division of Engineering ATTN: R. Clifton J. Duffy B. Freund A. Needleman R. Asaro Providence, RI 02912

No of Copies	Organization
1	Brown University Division of Applied Mathematics ATTN: C. Dafermos Providence, RI 02912
2	Carnegie-Mellon University Dept. of Mathematics ATTN: D. Owen M. Gurtin Pittsburg, PA 15213
6	Cornell University Dept. of Theoretical and Applied Mechanics ATTN: Y. Pao J. Jenkins P. Rosakis W. Sachse T Healey A. Zehnder Ithaca, NY 14850
2	Harvard University Division of Engineering and Applied Physics ATTN: J. Rice J. Hutchinson Cambridge, MA 02138
2	Iowa State University Engineering Research Laboratory ATTN: A. Sedov G. Nariboli Ames, IA 50010
2	Lehigh University Center for the Application of Mathematics ATTN: E. Varley R. Rivlin Bethlehem, PA 18015
1	North Carolina State University Dept. of Civil Engineering ATTN: Y. Horie Raleigh, NC 27607
1	Rice University Dept. of Mathematical Sciences ATTN: C.-C. Wang P.O. Box 1892 Houston, TX 77001
3	The Johns Hopkins University Dept. of Mechanical Engineering Latrobe Hall ATTN: W. Sharp R. Green A. Douglas 34th and Charles Streets Baltimore, MD 21218
1	Tulane University Dept. of Mechanical Engineering ATTN: S. Cowin New Orleans, LA 70112

No of Copies	Organization
1	University of California at Santa Barbara Dept. of Materials Science ATTN: A. Evans Santa Barbara, CA 93106
5	University of California at San Diego Dept. of Applied Mechanics and Engineering Sciences ATTN: S. Nemat-Nasser M. Meyers G. Ravichandran X. Markenscoff A. Hoger La Jolla, CA 92093
1	Northwestern University Dept. of Applied Mathematics ATTN: W. Olmstead Evanston, IL 60201
4	University of Florida Dept. of Engineering Science and Mechanics ATTN: L. Malvern D. Drucker E. Walsh M. Eisenberg Gainesville, FL 32601
2	University of Houston Dept. of Mechanical Engineering ATTN: L. Wheeler R. Nachlinger Houston, TX 77004
2	University of Illinois Dept. of Theoretical and Applied Mechanics ATTN: D. Carlson D. Stewart Urbana, IL 61801
2	University of Illinois at Chicago Circle Dept. of Engineering, Mechanics, and Metallurgy ATTN: T. Ting D. Krajcinovic P.O. Box 4348 Chicago, IL 60680
2	University of Kentucky Dept. of Engineering Mechanics ATTN: M. Beatty O. Dillon, Jr. Lexington, KY 40506
1	University of Kentucky School of Engineering ATTN: R. Bowen Lexington, KY 40506

No of Copies	Organization
2	University of Maryland Dept. of Mathematics ATTN: S. Antman T. Liu College Park, MD 20742
3	University of Minnesota Dept. of Aerospace Engineering and Mechanics ATTN: J. Erickson R. Fosdick R. James 110 Union Street SE Minneapolis, MN 55455
2	University of Oklahoma School of Aerospace, Mechanical and Nuclear Engineering ATTN: A. Khan C. Bert Norman, OK 73019
4	University of Texas Dept. of Engineering Mechanics ATTN: M. Stern M. Bedford J. Oden Austin, TX 78712
1	University of Washington Dept. of Aeronautics and Astronautics ATTN: J. Fife 206 Guggenheim Hall Seattle, WA 98195
2	University of Maryland Dept. of Mechanical Engineering ATTN: R. Armstrong J. Dally College Park, MD 20742
1	University of Wyoming Dept. of Mathematics ATTN: R. Ewing P.O. Box 3036 University Station Laramie, WY 82070
3	Washington State University Dept. of Physics ATTN: R. Fowles G. Duvall Y. Gupta Pullman, WA 99163
1	Yale University Dept. of Mechanical Engineering ATTN: E. Onat 400 Temple Street New Haven, CT 96520

No of Copies	Organization
1	Institute for Defense Analysis ATTN: G. Mayer 1801 N. Beauregard Street Alexandria, VA 22311
1	Honeywell, Inc. Defense Systems Division ATTN: G. Johnson 600 Second Street NE Hopkins, MN 55343
7	SRI International ATTN: D. Curran R. Shockey L. Seaman D. Erlich A. Florence R. Caliguri H. Giovanola 333 Ravenswood Avenue Menlo Park, CA 94025
1	Southwest Research Institute Department of Mechanical Sciences ATTN: U. Lindholm 8500 Culebra Road San Antonio, TX 02912
1	Commander US Army Research and Standardization Group (Europe) ATTN: F. Oertel P.O. Box 65 FPO, NY 09510

INTENTIONALLY LEFT BLANK.

USER EVALUATION SHEET/CHANGE OF ADDRESS

This Laboratory undertakes a continuing effort to improve the quality of the reports it publishes. Your comments/answers to the items/questions below will aid us in our efforts.

1. BRL Report Number BRL-MR-3807 Date of Report JANUARY 1990

2. Date Report Received _____

3. Does this report satisfy a need? (Comment on purpose, related project, or other area of interest for which the report will be used.) _____

4. How specifically, is the report being used? (Information source, design data, procedure, source of ideas, etc.) _____

5. Has the information in this report led to any quantitative savings as far as man-hours or dollars saved, operating costs avoided or efficiencies achieved, etc? If so, please elaborate. _____

6. General Comments. What do you think should be changed to improve future reports? (Indicate changes to organization, technical content, format, etc.)

_____

_____

_____

CURRENT ADDRESS

_____
Name

_____
Organization

_____
Address

_____
City, State, Zip

7. If indicating a Change of Address or Address Correction, please provide the New or Correct Address in Block 6 above and the Old or Incorrect address below.

OLD ADDRESS

_____
Name

_____
Organization

_____
Address

_____
City, State, Zip

(Remove this sheet, fold as indicated, staple or tape closed, and mail.)

— — — — — — — — — — FOLD HERE — — — — — — — — — —

Director
U.S. Army Ballistic Research Laboratory
ATTN: SLCBR-DD-T
Aberdeen Proving Ground, MD 21005-5066

NO POSTAGE
NECESSARY
IF MAILED
IN THE
UNITED STATES

OFFICIAL BUSINESS

BUSINESS REPLY MAIL
FIRST CLASS PERMIT NO 12062 WASHINGTON, DC

POSTAGE WILL BE PAID BY DEPARTMENT OF THE ARMY

Director
U.S. Army Ballistic Research Laboratory
ATTN: SLCBR-DD-T
Aberdeen Proving Ground, MD 21005-9989

— — — — — — — — — — FOLD HERE — — — — — — — — — —